

Fig. 9. Surface creep and saltation.

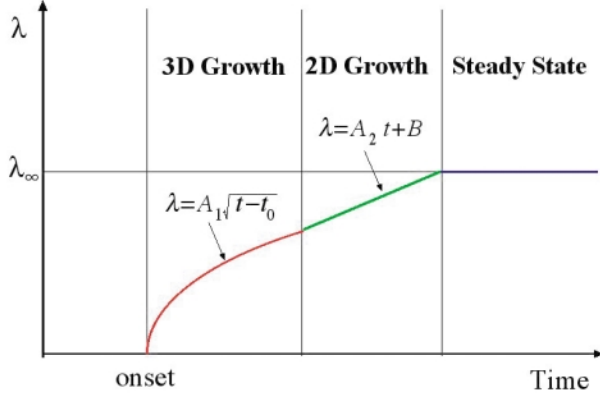


Fig. 10. Three regime growth model.

of height y_0 with the above terminal velocity is estimated to be

$$x_0 = \frac{6\pi\mu a y_0}{\Delta m g} U_x = \frac{9\mu y_0}{2a^2 \Delta \rho g} U_x, \quad (16)$$

from which we can estimate the wavelength $\lambda \approx 2x_0$.

Thus it is anticipated that the wavelength is

- 1) shorter for heavier particle,
- 2) shorter for larger particle,
- 3) longer in more viscous fluid,
- 4) longer for faster flow,
- 5) proportional to the wave height.

4.4 Comparison with experiment

Our models are schematically described in Fig. 10. The wavelength and wave width data shown in Figs. 5(a)–(c) are plotted in logarithmic scale in Fig. 11, which seem to agree with the square-root growth in the initial stage in spite of some scattering of the data. Apparently the side wall of the container restricts the dimension of horizontal spread. Closer look of the ripple formation, however, reveals that the boundary is not as clearly defined as the solid wall. Indeed, the inner side of the ripples are limited by the natural boundary of the undulation of the granular surface associated with the decrease of velocity due to the boundary layer (see e.g., Fig. 2), which is also the case near the outer cylindrical wall. Thus the side boundaries of the surface undulation are not directly limited by the solid walls, but rather by the velocity distribution. As has been reported (Hori *et al.*, 2007), horizontal velocity distribution in our annular channel is an almost linearly increasing function across the channel width accompanied by the boundary layer near the

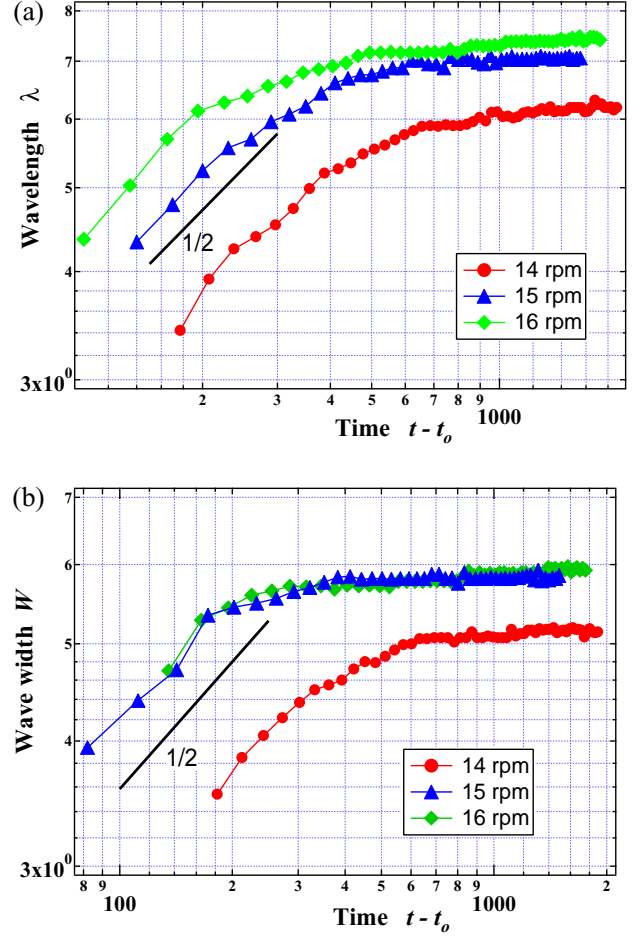


Fig. 11. Initial Growth of the wavelength (a) and wave width (b) in log-log plot.

walls. The latter distribution causes faster movement of the ripple in outer part of the ridges, which results in obliquely arranged ripples, and hence partially overlapped ripples in the circumferential direction (see Fig. 2(b)). This overlapping is enhanced in slower flow, which makes difficult to observe 2D growth range in Figs. 5(a) and (b). On the other hand, the intermediate region is recognized in Fig. 5(c), which duly results in poorer agreement in the exponential fitting curve of Fig. 5(c) and non-monotonic behavior of mode 3 in Fig. 6(c).

We have as yet no data to check the anticipation (1)–(3) of Subsec. 4.3, because all the data were obtained using glass beads of a single diameter in a particular fluid (water),